Supplementary Information

Tuning contact properties in $MoSi_2N_4$ van der Waals heterostructures with Janus metals: Realizing Ohmic contacts

Shiying Guo*, Siqi Yang, Ying Wang, Chen Zhuang, Han Li, Jing Pan*

College of Physics Science and Technology, Yangzhou University, Yangzhou 225002, China

E-mail:

*guosy@yzu.edu.cn

*jp@yzu.edu.cn

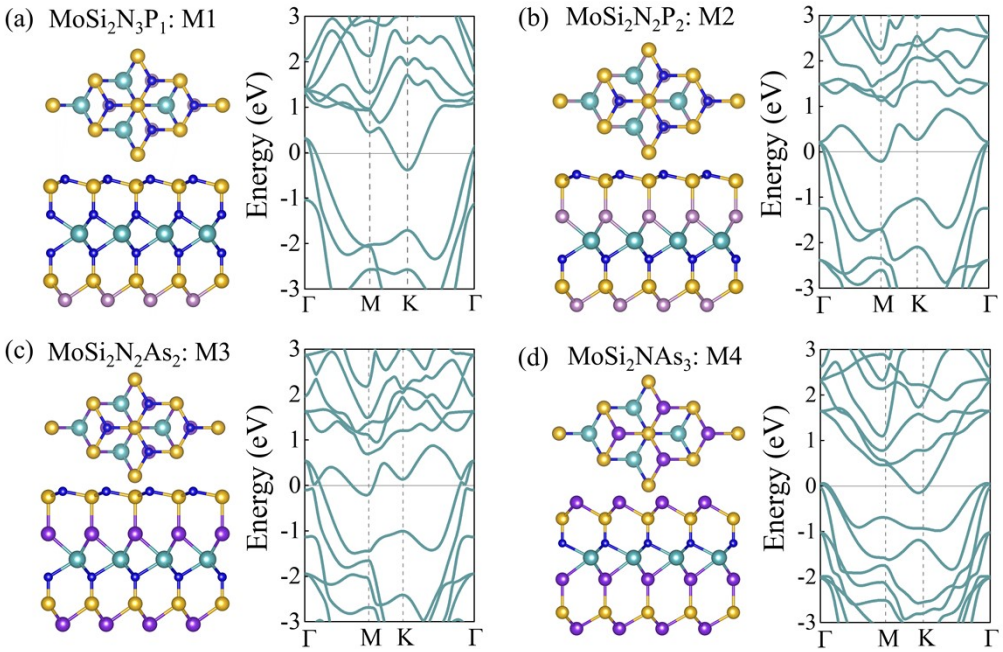

Fig. S1 Top and side views of the atomic structure and band structure of (a) $MoSi_2N_3P_1$, (b) $MoSi_2N_2P_2$, (c) $MoSi_2N_2As_2$, and (d) $MoSi_2NAs_3$ monolayers. They are represented by M1, M2, M3 and M4, respectively.

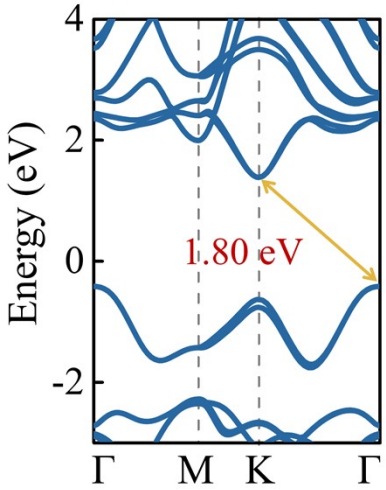

Fig. S2 The band structure of $MoSi_2N_4$ (MSN) with spin-orbit coupling (SOC).

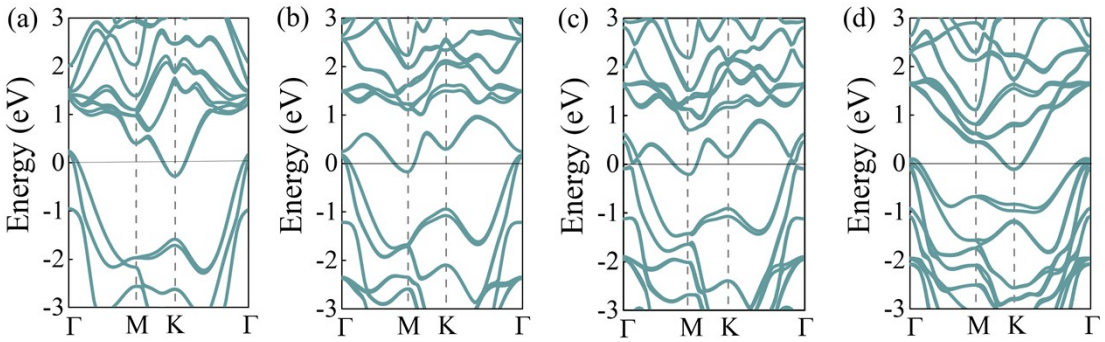

Fig. S3 Band structures of the four Janus metal monolayers with SOC: (a) M1, (b) M2, (c) M3, and (d) M4.

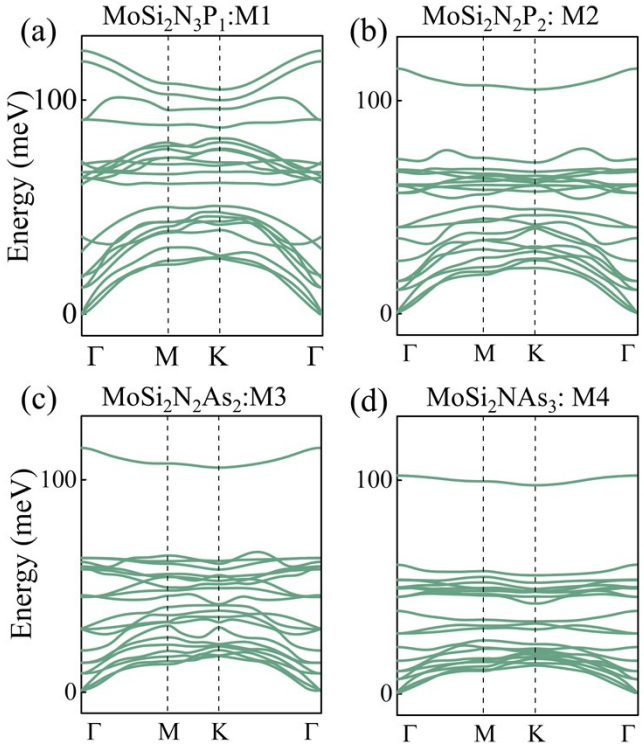

Fig. S4 Phonon dispersion spectrum of (a) M1, (b) M2, (c) M3, and (d) M4 monolayers.

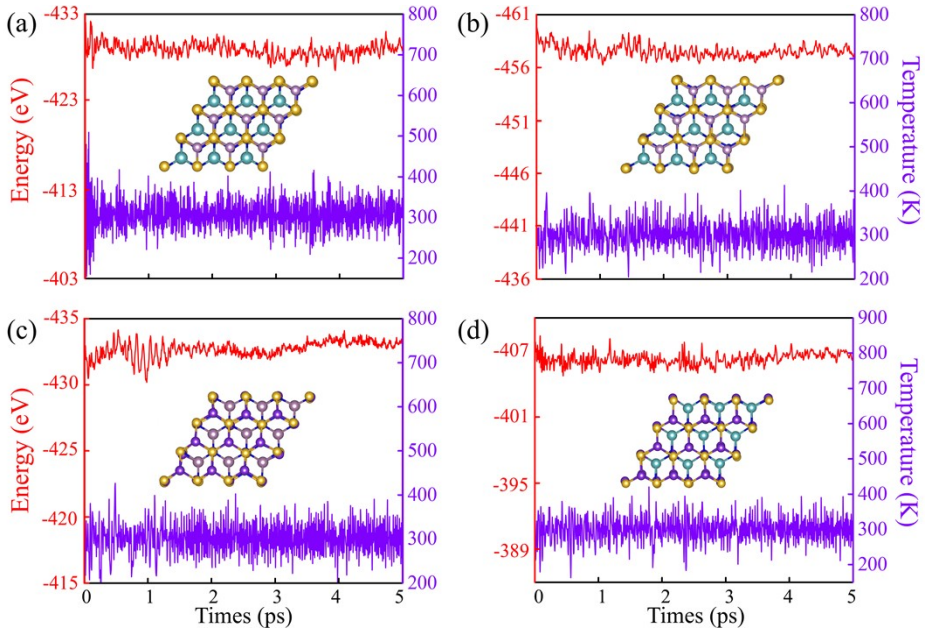

Fig. S5 Total energy and temperature during an ab initio molecular dynamics (AIMD) simulation of (a) M1, (b) M2, (c) M3, and (d) M4 at 300 K. Inset: atomic structure after 5 ps.

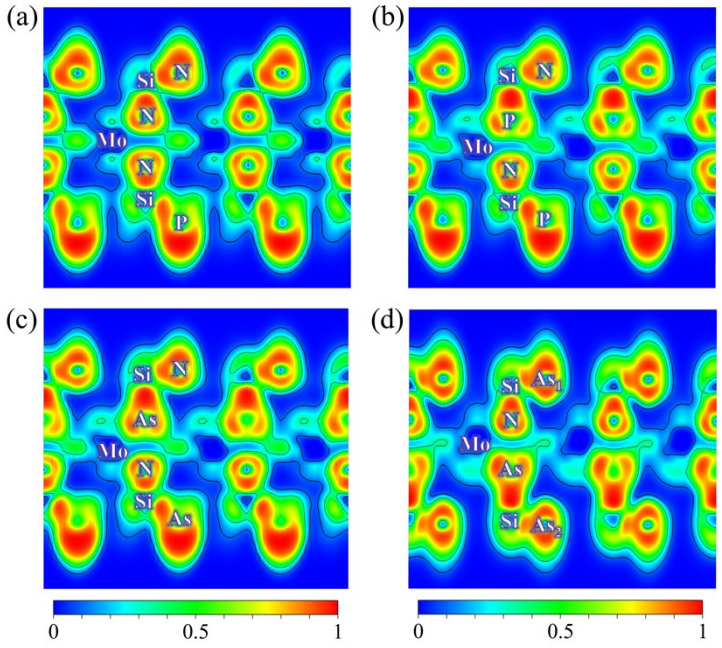

Fig. S6 Electronic localization function (ELF) of (a) M1, (b) M2, (c) M3, and (d) M4, respectively.

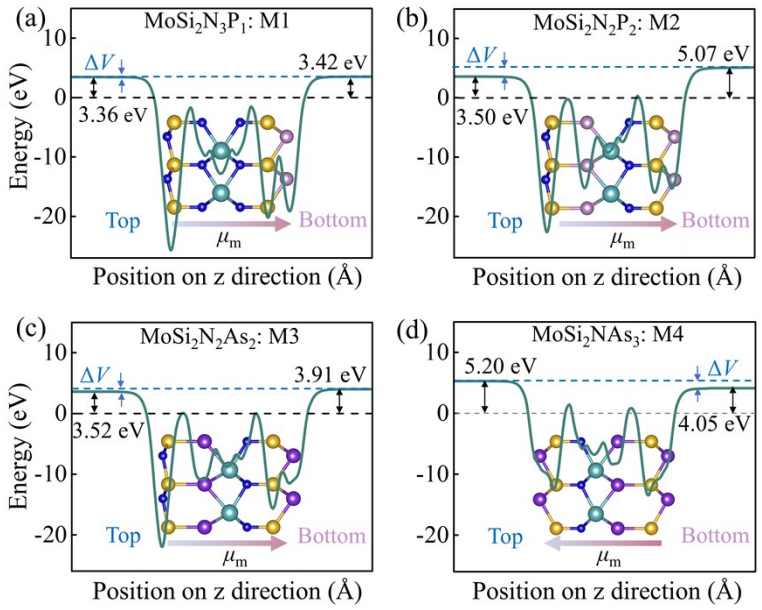

Fig. S7 Plane-averaged electrostatic potentials of (a) M1, (b) M2, (c) M3, and (d) M4 monolayers.

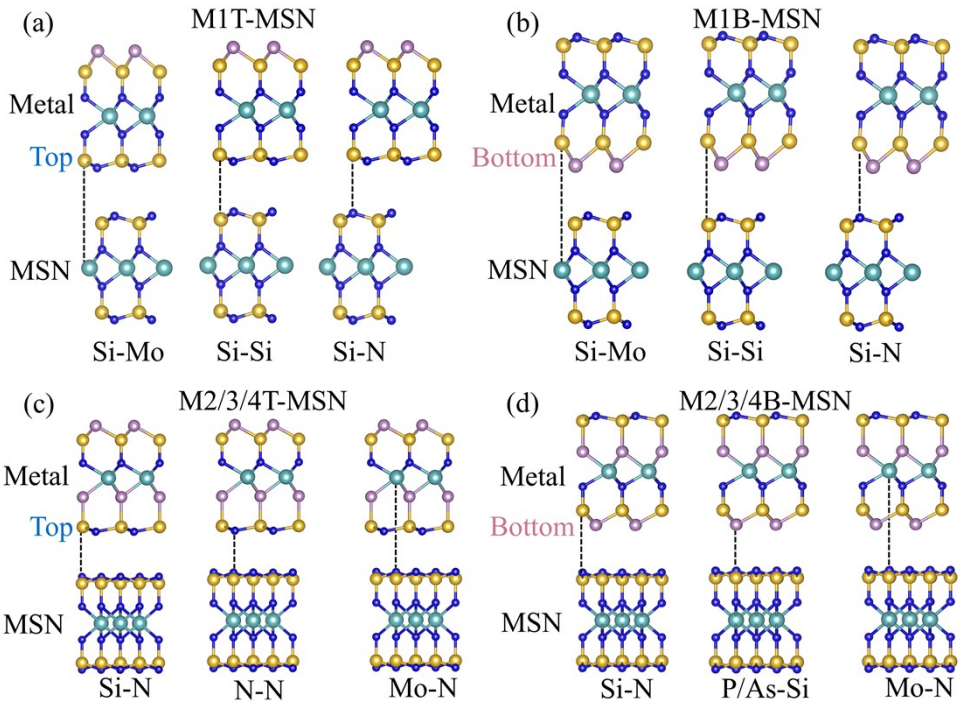

Fig. S8 Different types of interfacial stacking modes for M1T-MSN, M1B-MSN, M2/3/4T-MSN, and M2/3/4B-MSN.

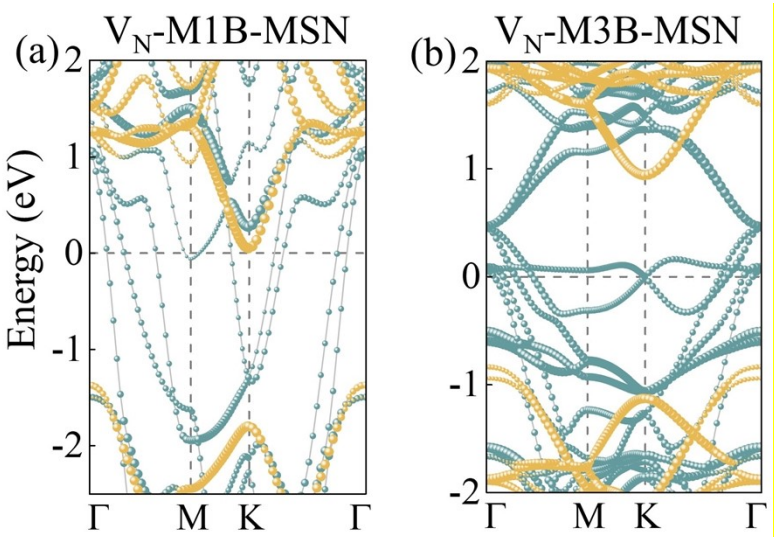

Fig. S9 Projected band structure of (a) V_N-M1B-MSN and (b) V_N-M3B-MSN heterostructures. The sand yellow and dark cyan spheres represent the contributions from MSN and 2D Janus metals, respectively. The weighted contribution is described by the size of the spheres. The Fermi level is set to 0 eV.

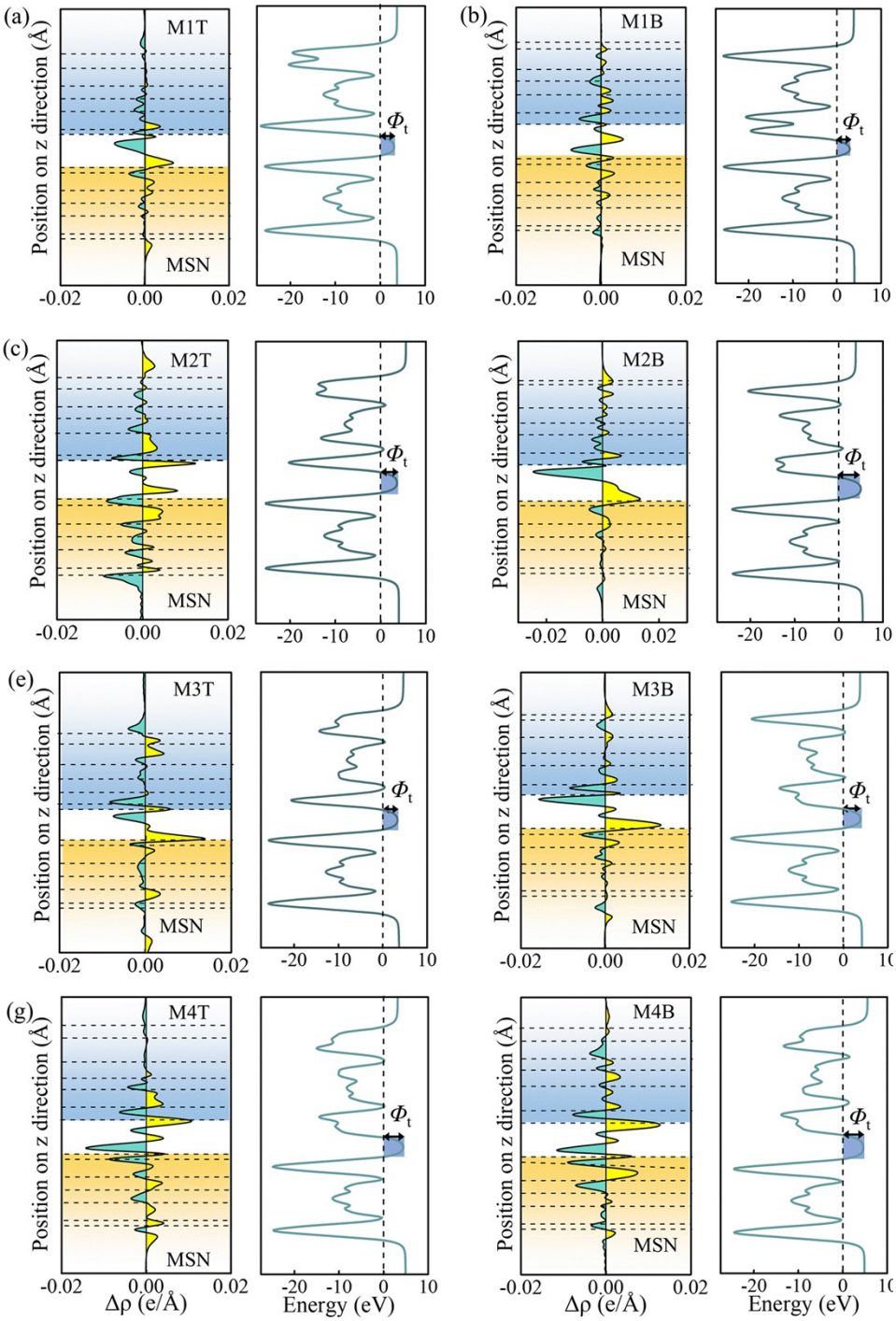

Fig. S10 Plane-averaged electron density difference and plane-averaged electrostatic potentials of (a) M2T-MSN, (b) M2B-MSN, (c) M2T-MSN, (d) M2B-MSN, (e) M3T-MSN, and (f) M4B-MSN vdW MSJs.

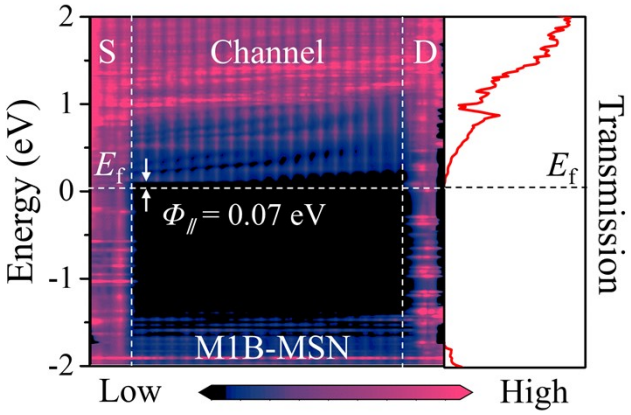

Fig. S11 Projected local density of states (PLDOS) and transmission spectrum of M1B-MSN FET under zero bias voltage with SOC correction.

Table S1 Lattice constant (a), cohesive energy (E_{coh}), potential step (ΔV_m) between the top side and bottom side, and intrinsic dipoles (μ_m) of $MoSi_2N_3P_1$ (M1), $MoSi_2N_2P_2$ (M2), $MoSi_2N_2As_2$ (M3) and $MoSi_2NAs_3$ (M4) monolayers.

2D-metal	a (Å)	E_{coh} (eV/atom)	ΔV_m (eV)	μ_m (D)
M1	2.90	−7.65	−0.06	−0.038
M2	3.17	−6.92	−1.57	−0.350
M3	3.24	−6.58	−0.39	−0.096
M4	3.53	−7.43	1.15	0.320

Table S2 Bond lengths of P/As-Si in 2D Janus metals and the sum of the covalent radius (R) of P/As and Si atoms.

bond	bond length (Å)	R (Å)
P-Si	2.24	2.28
P-Si	2.17	2.28
As-Si	2.29	2.40
As_1-Si	2.06	2.40
As_2-Si	2.06	2.40

Table S3 Dipole moments (μ'_m) and work functions (W'_F) of 2D Janus metals under the inevitable lattice mismatch-induced strain (ε).

2D-metal	ε (%)	μ'_m (D)	W'_F (eV)	
			Top	Bottom
M1	0.00	−0.038	3.36	3.42
M2	5.24	−0.380	3.67	5.15
M3	3.24	−0.078	3.62	3.92
M4	5.03	0.300	5.03	4.07

Table S4 Lattice mismatch (ε), binding energy (E_b), charge transfer (Q) per metal unit cell to MSN, and interlayer distance (d) of 2D vdW MSJs. A positive charge transfer value indicates electron transfer from the metal to the MSN.

vdW MSJs	ε (%)	E_b (eV/Å^2)	Q (e)	d (Å)
M1T-MSN	0.00	−0.018	0.001	3.25
M1B-MSN	0.00	−0.020	−0.001	3.24
M2T-MSN	5.24	−0.039	0.009	3.39
M2B-MSN	5.24	−0.034	0.012	3.48
M3T-MSN	3.24	−0.036	0.004	3.12
M3B-MSN	3.24	−0.030	0.006	3.42
M4T-MSN	5.03	−0.011	−0.007	3.39
M4B-MSN	5.03	−0.010	−0.010	3.40

Table S5 The n-type SBH (Φ_{Bn}), p-type SBH (Φ_{Bp}), the tunnel barrier width (ω_t), the tunnel barrier height (Φ_t), and the tunneling probability (P_{TB}) of the 2D vdW MSJs.

vdW MSJs	Φ_{Bn} (eV)	Φ_{Bp} (eV)	ω_t (Å)	Φ_t (eV)	P_{TB} (%)
M1T-MSN	0.35	1.38	1.42	3.16	7.54
M1B-MSN	−0.02	1.82	1.16	3.01	12.74
M2T-MSN	0.26	1.59	1.59	3.68	4.40
M2B-MSN	1.78	0.04	1.79	5.04	1.63
M3T-MSN	0.65	1.19	1.49	3.40	6.00
M3B-MSN	0.63	1.19	1.50	3.93	4.76
M4T-MSN	0.83	0.99	1.44	4.50	4.38
M4B-MSN	0.29	1.52	1.98	4.69	1.24

Table S6 The n-type SBH (Φ_{Bn}) and p-type SBH (Φ_{Bp}) of 2D M1B-MSN and M3B-MSN heterostructures containing N vacancies.

vdW MSJs	Φ_{Bn} (eV)	Φ_{Bp} (eV)
V_N-M1B-MSN	0.04	/
V_N-M3B-MSN	0.94	0.84